Band-structure perturbations in strained crystals. II. Shifts at the Fermi surface of Cu

D. M. Gray and A. Marcus Gray
Physical Science Division, Benet Weapons Laboratory, Watervliet Arsenal, Watervliet, New York 12189
(Received 2 February 1976)

In a previous paper, we described the use of a perturbation technique in conjunction with the modified-plane-wave method to calculate first-order changes in electronic energy levels for fcc crystals under hydrostatic, tetragonal, and trigonal strains. In the present paper this approach is applied to changes at the Fermi level of Cu. We outline the use of these shifts to estimate changes in extremal Fermi-surface areas which may then be compared with de Haas–van Alphen data. Results for the hydrostatic case compare reasonably well with other calculations and with observation. For the uniaxial-stress cases comparison is made with the calculation of Davis and with observation by taking the appropriate linear combination of our hydrostatic and tetragonal (trigonal) results. Reasonable agreement with the limited experimental values is obtained; agreement with Davis is reasonably good in two cases but poor in others.

I. INTRODUCTION

In a previous paper,[1] hereafter referred to as I, a perturbation procedure was developed within the framework of the modified-plane-wave formalism to calculate first-order shifting and splitting of electronic energy levels for fcc crystals under hydrostatic, tetragonal, and trigonal strains. Numerical results for Cu for several high-symmetry points were given. We have now[2] applied the procedure to calculate shifts at the Fermi level of Cu. From these shifts one may compute the change in area perpendicular to certain directions and compare with de Haas–van Alphen measurements.

The one-electron potential used is described in Sec. II. The use of symmetry to simplify the shear-strain calculations is discussed in Sec. III while Sec. IV describes some preliminary tests. Strain-induced energy shifts near the Fermi level are given in Sec. V; use of these energy shifts to compute changes in orbital area is outlined in Sec. VI. In Sec. VII we make some brief comments on a different Cu potential. Major points are summarized in Sec. VIII.

II. THE POTENTIAL

The Cu potential used is taken from Davis, Faulkner, and Joy[3] (DFJ). These authors used the Löwdin-Mattheiss prescription[4] to generate crystal potentials for a, $0.995a$, and $0.99a$, where a is the normal lattice constant. The DFJ crystal potential is based on atomic Hartree-Fock wave functions (calculated by Watson[5] for a $3d^9 4s^2$ configuration) inserted into a $3d^{10}4s$ configuration. DFJ had previously calculated Cu band structures for this and for two other potentials; the potential based on the Watson functions was chosen as, of the three tested, it gave the most satisfactory agreement with the experimentally established unperturbed Cu band structure.

The change in potential associated with hydrostatic strain is obtained from

$$\Delta V(r) = V_{(1+e)a}(r) - V_a(r) \tag{1}$$

for the value within the muffin-tin spheres; the interstitial value is given by

$$\Delta \overline{V} = \overline{V}_{(1+e)a} - \overline{V}_a \ . \tag{2}$$

DFJ used a radial integration mesh of 272 points; we interpolated their potential onto a 66-point mesh.[6] As a preliminary test we calculated energy levels and hydrostatic strain shifts for some selected $\vec{k}$ points using both meshes; the differences in E^0 were appreciable (up to 0.02 Ry) whereas the differences in energy *shifts* were small (maximum of 3×10^{-5} Ry for $e=-0.005$). Since we are primarily concerned here with energy shifts and since most of the hydrostatic strain shifts calculated for $e=-0.005$ are $\sim10^{-3}$ or larger, the discrepancy between the two mesh values is not particularly important. All shifts reported in this paper refer to the 66-point mesh unless explicitly labeled otherwise. The lattice constant used is 6.830 90 Bohr radii[7]; this is the same as used by DFJ. The radius of the muffin-tin sphere was chosen as 2.400 Bohr radii; this allows compression to $0.995a$ without causing overlap of the spheres.

III. SYMMETRY CONSIDERATIONS

For the hydrostatic case there is, of course, no change in crystal symmetry. For the shear strains, however, there is a lowering of the cubic symmetry. It is well known[8,9] that it is this change of symmetry which makes the shear strains a particularly critical test of the original potential. In the usual shear strain experiment one employs a

uniaxial stress, applying tension in the z direction, say, and allowing the elastic constants to dictate the deformation in the x and y directions. Such a strain corresponds (to first order) to a unique combination of hydrostatic and tetragonal strains (or hydrostatic and trigonal if a uniaxial $\langle 111 \rangle$ stress is employed).

In the Appendix we show that for cubic crystals under a volume-preserving strain, both the Fermi level and the sum over a "star of $\vec{k}$" of any given level belonging to any given irreducible representation remain unchanged to first order. As shown in I, this allows one to make a number of predictions regarding *ratios* of shifts from symmetry considerations alone. If a model is chosen which constrains the potential to spherical symmetry within a muffin-tin sphere (after deformation as well as before) the discussion in the Appendix shows that the statement above applies to $V(r)$ also. Since this "muffin-tin condition" on the potential holds in our model, the band-structure shifts and splittings in the tetragonal and trigonal strain cases are due solely to the change in symmetry and to the *explicit* change in lattice constant, i.e., there is only a "geometric" effect but no "potential" effect [change in band structure due to the change in $V(r)$ caused by the change in lattice constant].

IV. PRELIMINARY TESTS

A. Hydrostatic

As a preliminary test we calculated energy levels and shifts under hydrostatic strain for some selected high-symmetry points and compared with the corresponding DFJ values; results are tabulated in Table I. For comparison, this table also lists: (i) Our perturbation results obtained by using the Chodorow potential[10] for $V_0(r)$ in conjunction with the $\Delta V(r)$ of DFJ. (ii) The difference-calculation results of O'Sullivan *et al.*[11] As far as possible all cubic symmetry states are labeled in the Bouckaert-Smoluchowski-Wigner (BSW) notation.[12] The E^0 values listed in Table I are higher than those found by DFJ[3]; the d-type states ($\Gamma_{12}, \Gamma_{25'}, X_5, L_3$) are as much as 0.02 to 0.03 Ry higher. As noted earlier, we do *not* feel this causes appreciable errors in ΔE since on going to the 272-point mesh E^0 drops to within about 0.01 Ry of the DFJ values without any appreciable change in ΔE; the same effect is noted if one calculates E^0 and ΔE for a given level and then simply repeats the calculation using more symmetrized plane waves in the trial expansion function, i.e., ΔE "converges" much more rapidly than E^0.

For most levels agreement between our perturbation results and the DFJ difference calculation improved, as one would expect, when the perturbation calculation used the DFJ $V_0(r)$; note particularly $\Gamma_1, X_{4'}$ and $L_{2'}$. The X_5 and L_3^u discrepancies remain the same.[13] [The one level with an *increased* discrepancy (L_1^u) differs only slightly between all three calculations.] We note that for the p-type states ($X_{4'}, L_{2'}$) the Chodorow-based perturbation calculation agrees very well with the Herman-Skillman-based difference calculation (column 6); we have not pursued the reasons for this agreement.

B. Tetragonal

Our perturbation program for tetragonal (and trigonal) shear strains has been tested in I by comparing our results with those of Juras and Segall[14]; the Chodorow potential was used. Agreement was reasonably good.

As a further test, we compared our results for some selected high-symmetry points with the uniaxial $\langle 001 \rangle$ results of Davis.[15] To first order one may represent the Davis uniaxial $\langle 001 \rangle$ tension ($e_{zz} = 0.02500$, $e_{xx} = e_{yy} = -0.010372$)[16] by a linear combination of our hydrostatic and tetragonal strains (assuming linearity for the hydrostatic case in this range). The combination required is

$$\Delta E_{\langle 001 \rangle} = -0.2838 \Delta E_h + 23.581 \Delta E_t \ , \tag{3}$$

where ΔE_h is our hydrostatic ΔE for $e = -0.005$ and ΔE_t is our tetragonal ΔE for $e_{zz} = 0.001$. This comparison is given in Table II; considering the uncertainties and the linear approximation made, agreement is reasonably good.

C. Trigonal

Proceeding as above one may represent the Davis[15] uniaxial $\langle 111 \rangle$ tension ($e_{xx} = e_{yy} = e_{zz} = 0.01000$, $e_{xy} = e_{xz} = e_{yz} = 0.02605$) by the linear combination

$$\Delta E_{\langle 111 \rangle} = -2.0 \Delta E_h + 26.051 \Delta E_{\rm tr} \ , \tag{4}$$

where ΔE_h is again our hydrostatic ΔE for $e = -0.005$ and $\Delta E_{\rm tr}$ is our trigonal ΔE for $e_{xy} = e_{xz} = e_{yz} = 0.001$. This comparison is given in Table III. Agreement here is not as good as in the tetragonal case.

D. Discussion of energy shifts

For hydrostatic compression one expects a general broadening of the electronic energy bands. For shear strains, however, some pairs of atoms move closer together while other pairs move apart; one thus expects a mixed effect on the electronic bands. This is indicated in our results if one considers $W_d(X) \equiv X_5 - X_1$ and $W_d(L) \equiv L_3^u - L_1^l$ as

TABLE I. Shifts in energy for some high-symmetry states of Cu for hydrostatic compression ($e = \Delta a/a = -0.005$). All energies are in Ry.

State [a]	E^0	ΔE Perturbation [Chodorow $V_0(r)$] [b]	ΔE Perturbation [DFJ $V_0(r)$] [b]	ΔE by differences DFJ [c]	ΔE by differences OSSS [d]
Γ_{12}	−0.600	−0.0020	−0.0023	−0.0028	−0.0032
$\Gamma_{25'}$	−0.658	−0.0035	−0.0038	−0.0042	−0.0047
Γ_1	−1.141	−0.0109	−0.0095	−0.0097	−0.0155
$X_{4'}$	−0.345	−0.0032	−0.0018	−0.0018	−0.0030
X_5	−0.546	−0.0010	−0.0010	−0.0016	−0.0019
L_1^u	−0.162	0.0045	0.0048	0.0046	0.0040
$L_{2'}$	−0.553	−0.0058	−0.0046	−0.0046	−0.0058
L_3^u	−0.554	−0.0013	−0.0013	−0.0019	−0.0022
L_3^l	−0.660	−0.0037	−0.0040	−0.0043	−0.0049
L_1^l	−0.811	−0.0075	−0.0068	−0.0071	−0.0079

[a] BSW labels (Ref. 12). The superscripts u and l indicate upper and lower levels, respectively. The E^0 values listed are for the DFJ potential (our calculation) are are primarily for identification. The corresponding E^0 values for the Chodorow potential are considerably higher.

[b] Both perturbation calculations used the $\Delta V(r)$ of DFJ.

[c] Reference 3.

[d] Reference 11. Table I of this reference lists Cu shifts corresponding to $e = -0.024$; for incorporation into our table we have adjusted their results by multiplying by 0.005/0.024, i.e., we have assumed linearity with e.

"width" of the d band at X and L, respectively; similarly we take $W_{sp}(\Gamma X) \equiv X_{4'} - \Gamma_1$ and $W_{sp}(\Gamma L) \equiv L_{2'} - \Gamma_1$ as "width" of the "sp-band" in the ΓX and ΓL directions, respectively. Values for the changes in these "widths" are given in Table IV. As expected, the widths are increased under hydrostatic compression. For the sp-band under shear there is broadening for $\vec{k}$-space directions (tetragonal ⟨100⟩, trigonal $\langle 1\bar{1}1\rangle$) corresponding to directions which are compressed in real space and narrowing for directions (tetragonal ⟨001⟩, trigonal ⟨111⟩) corresponding to directions which are stretched in real space. For the d band $|\Delta W|$ under shear is relatively small; the expected broadening for the compressed real space direc-

TABLE II. Energy shifts for some high-symmetry states of Cu for uniaxial ⟨001⟩ tension ($e_{zz} = 0.02500$, $e_{xx} = e_{yy} = -0.010372$). Column 2 is a linear combination of our hydrostatic and tetragonal strains chosen to match the uniaxial case [see Eq. (3) of text]. All shifts are in Ry.

State	ΔE Eq. (3)	ΔE [a] Uniaxial ⟨001⟩
Γ_{12}	0.0066	0.0069
	−0.0053	−0.0050
$\Gamma_{25'}$	0.0048	0.0053
	−0.0064	−0.0056
Γ_1	0.0027	0.0025
$X_{4'}$ (001)	−0.0388	−0.0380
(100)	0.0202	0.0206
X_5 (001)	−0.0004	−0.0001
(100)	0.0051	0.0055
(100)	−0.0037	−0.0032
X_1 (001)	0.0006	0.0009
(100)	0.0029	0.0029
L_3^u	0.0031	0.0032
	−0.0024	−0.0015
L_1^l	0.0019	0.0021

[a] Reference 15.

TABLE III. Energy shifts for some high-symmetry states of Cu for uniaxial ⟨111⟩ tension ($e_{xx} = e_{yy} = e_{zz} = 0.01\,000$, $e_{xy} = e_{xz} = e_{yz} = 0.02\,605$). Column 2 is a linear combination of our hydrostatic and trigonal strains chosen to match the uniaxial case [see Eq. (4) of text]. All shifts are in Ry.

State	ΔE Eq. (4)	ΔE [a] Uniaxial ⟨111⟩
Γ_{12}	0.0047	0.0060
$\Gamma_{25'}$	0.0180	0.0135
	−0.0133	−0.0125
Γ_1	0.0191	0.0143
$X_{4'}$	0.0037	0.0022
X_3	0.0125	0.0099
$L_{2'}(\frac{1}{2}\frac{1}{2}\frac{1}{2})$	−0.0545	−0.0535
$(\frac{1}{2}\frac{\bar{1}}{2}\frac{1}{2})$	0.0304	0.0264
$L_3^u(\frac{1}{2}\frac{1}{2}\frac{1}{2})$	−0.0039	−0.0021
$L_3^l(\frac{1}{2}\frac{1}{2}\frac{1}{2})$	0.0144	0.0117

[a] Reference 15.

TABLE IV. d and "sp" bandwidth changes for hydrostatic, tetragonal, and trigonal strains. See text for definition of column headings. A positive entry indicates broadening; a negative entry, narrowing. All width changes are in Ry.

	$\Delta W_{sp}(\Gamma X)$	$\Delta W_{sp}(\Gamma L)$	$\Delta W_d(X)$	$\Delta W_d(L)$
hydrostatic [a]	0.0077	0.0050	0.0063	0.0055
tetragonal [b]	(001) −0.0084	(all L) 0.0 [d]	(001) 0.0002	(all L) 0.0006
	(100) 0.0042		(100) 0.0009	
trigonal [c]	(all X) 0.0 [d]	(111) −0.0122	(all X)0.0000(4)	(111) −0.0003
		(1$\bar{1}$1) 0.0040		(1$\bar{1}$1) 0.0019

[a] $e = -0.005$.
[b] $e_{zz} = 0.005$, $e_{xx} = e_{yy} = -0.0025$.
[c] $e_{xy} = e_{xz} = e_{yz} = 0.005$.
[d] These values are zero by symmetry.

tions shows up and $W_d(L)$ for the stretched ⟨111⟩ direction shows a very slight narrowing; $W_d(X)$, however, actually shows a very small broadening for the stretched ⟨001⟩ direction.

V. ENERGY SHIFTS NEAR E_F

A. Hydrostatic

Rather than calculate energy levels for the large number of $\vec{k}$ points required to obtain a realistic value of E_F, we have simply used the E_F of the DFJ calculation (Table III of Ref. 3 gives $E_F = -0.4678$ Ry). We also take k_F from DFJ; values for the ⟨100⟩, ⟨110⟩ directions and the [111] necks are given in Table V.

Energy shifts for a hydrostatic strain of $e = -0.005$ are given in Table VI for the k_F values listed in Table V. The DFJ values are given for comparison. Considering that a graphical interpolation has been made to extract the ΔE values from Ref. 3, agreement is quite good except for the neck. It is noted that the Δ_1 shift and the neck shifts are of comparable size while the Σ_1 shift is much smaller. It is also noted that the neck shifts for Q^- and P^+ symmetry are identical.

B. Tetragonal

We choose a tetragonal strain which singles out the z axis. For this choice ΔE for Δ_1 in the ⟨100⟩ and ⟨010⟩ directions will be $-\frac{1}{2}\Delta E$ of the ⟨001⟩ direction; similarly, ΔE for Σ_1 directions in the xz and yz planes will be $-\frac{1}{2}\Delta E$ for Σ_1 in the xy plane. For tetragonal strain all hexagonal faces will have identical ΔE behavior. On a given hexagonal face, however, ΔE for Q^- along Q directions labeled β (see Fig. 1) will be $-\frac{1}{2}\Delta E$ of the α directions; ΔE for P^+ along P directions labeled ω will be $-\frac{1}{2}\Delta E$ of the τ directions. The Q^- and P^+ lines which cross E_F each connect to $L_{2'}$. Since symmetry dictates that $L_{2'}$ must have $\Delta E = 0$ for tetragonal strain, one expects the ΔE values at k_F for Q^- and P^+ to be small. Energy shifts for tetragonal strain ($e_{zz} = 0.001$, $e_{xx} = e_{yy} = -0.0005$) are given in Table VII. The small value for Q^- confirms the expectation above (we did not calculate P^+).

C. Trigonal

For a trigonal strain which singles out the ⟨111⟩ axis ΔE for Σ_1 given by $(b, b, 0)$, $(b, 0, b)$, $(0, b, b)$, $(\bar{b}, \bar{b}, 0)$, $(\bar{b}, 0, \bar{b})$, and $(0, \bar{b}, \bar{b})$ will be identical; ΔE for the other six Σ directions will be $-\Delta E$ of the first set. ΔE for all Δ_1 levels must be zero from symmetry. The two hexagonal faces perpendicular to the ⟨111⟩ axis behave differently from the other six hexagonal faces which behave identically. All six Q lines in the face containing L at $(\frac{1}{2}, \frac{1}{2}, \frac{1}{2})$ behave identically; we designate any one of them as Q_α. For the "other type" hexagonal faces there will be two different-behavior Q lines; we designate these as Q_β and Q_γ (see Fig. 2). Symmetry considerations lead to the relation

TABLE V. k_F values for the unperturbed crystal in units of $2\pi/a_0$ for certain symmetry directions. These values [a] are taken from Table III of Ref. 3.

	k_x	k_y	k_z	k_{radius} [b]
k_F⟨001⟩	0.0	0.0	0.83302	0.83302
k_F⟨110⟩	0.52095	0.52095	0.0	0.73673
$k_F Q$ ⟨111⟩"neck"	0.6186	0.3814	0.5	0.16773
$k_F P$ [c] ⟨111⟩"neck"	0.43153	0.43153	0.63694	0.16773

[a] To convert the DFJ values to ours multiply the DFJ value by $(3/2\pi)^{1/3} = 0.781\,593$.
[b] For ⟨001⟩ and ⟨110⟩, k_{radius} is the distance from the origin of $\vec{k}$-space to k_F. For the neck, k_{radius} is the distance from the L point to k_F.
[c] This is a line from U (or K) to L; it may be expressed as $(0.25+b,\ 0.25+b,\ 1-2b)$ with $0 < b < 0.25$. There is no BSW label.

TABLE VI. Hydrostatic compression: Energy shifts at the Fermi level for $e=-0.005$ in $a=a_0(1+e)$. All energy shifts are in Ry.

Direction	State	k_{radius} [a]	ΔE Perturbation	ΔE by Differences [b]
⟨100⟩	Δ_1	0.83302	−0.0020	−0.0022
⟨110⟩	Σ_1	0.73673	0.0001	−0.0003
⟨111⟩ neck	Q^-	0.16773	−0.0019 [c]	−0.0024
⟨111⟩ neck	P^+	0.16773	−0.0019 [c]	

[a] Same meaning as in Table V; units of $2\pi/a_0$.
[b] Computed graphically from Table III of Ref. 3.
[c] The 272-point mesh was used. Q^- run with the 66-point mesh gave a similar ΔE value (−0.0017).

$$\Delta E(Q_\alpha^-)+\Delta E(Q_\beta^-)+2\Delta E(Q_\gamma^-)=0\ . \tag{5}$$

A similar relationship holds for P lines; designating any P line in the face containing L at $(\frac{1}{2},\frac{1}{2},\frac{1}{2})$ as P_ξ,

$$\Delta E(P_\xi^+)+\Delta E(P_\eta^+)+2\Delta E(P_\xi^+)=0\ , \tag{6}$$

with η and ξ directions as given in Fig. 2. Energy shifts for trigonal strain[16] ($e_{xy}=e_{xz}=e_{yz}=0.001$) are given in Table VIII.

VI. Δk_F and ΔA

In this section we describe the determination of the change in k_F and the change in the associated orbital area.

A. Hydrostatic strain

Given ΔE for k_F and for one or two values near k_F and a value for ΔE_F one may compute Δk_F graphically. To a fair approximation, one may also obtain the unscaled Δk_F from

$$\Delta k_F^{(u)}=-\left(\frac{dk}{dE}\right)_{E_F}(\Delta E-\Delta E_F)\ . \tag{7}$$

Here $(dE/dk)_{E_F}$ is the slope of E vs $\vec{k}$ near E_F in the unperturbed situation. When the change in scale on going from $2\pi/a_0$ to $2\pi/[a_0(1+e)]$ is taken into account one has (to first order),

$$\Delta k_F=\Delta k_F^{(u)}-ek_F\ . \tag{8}$$

Using $(dE/dk)_{E_F}$ and ΔE_F from DFJ and our values for ΔE we obtain Table IX. These values enable us to obtain a rough estimate of $(\Delta A/A)/\Delta P$ which may then be compared[17] with de Haas–van Alphen data.[18,19] It must be emphasized that we are estimating changes in extremal areas from a very small number of $\vec{k}$ directions; this is probably valid for the neck orbit which appears to be circular to a high degree but can only be roughly correct for the [001] belly. It is noted that a large number of $\vec{k}$ points and directions were used by DFJ. Resultant values are given in Table X. Considering the noncircularity of the belly orbit and the fact that only two symmetry directions in the orbit plane were used, our agreement with experiment may be partially fortuitous. The large

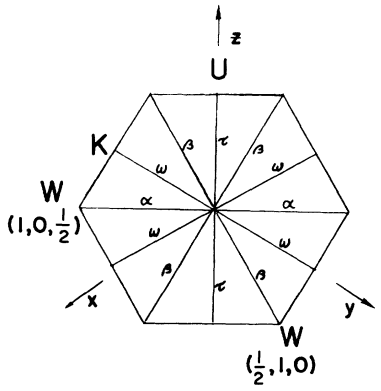

FIG. 1. Labeling of Q and P directions in a hexagonal face for ⟨001⟩ tetragonal strain. The L point at $(\frac{1}{2},\frac{1}{2},\frac{1}{2})$ is at the center of the hexagon. α,β designate Q lines; τ,ω designate P lines. All symmetry points are in units of $2\pi/a$.

TABLE VII. Tetragonal strain: Energy shifts at the Fermi level for $e=0.001$ in $a_z=a_0(1+e)$; $a_x=a_y=a_0(1-\frac{1}{2}e)$. See text to determine the symmetry-related shifts from those listed. All energy shifts are in Ry.

Direction	State [a]	k_{radius} [b]	ΔE Perturbation
⟨001⟩	Δ_1	0.83302	−0.0013
⟨110⟩	Σ_1	0.73673	0.0004
⟨111⟩ neck	Q_α^-	0.16773	−0.0000(2)

[a] For ⟨001⟩ tetragonal strain, the various directions in the hexagonal face normal to ⟨111⟩ are shown in Fig. 1.
[b] Same meaning as in Table V; units of $2\pi/a_0$.

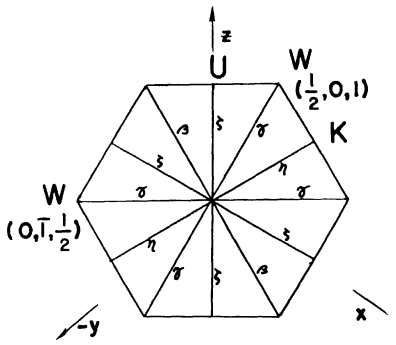

FIG. 2. Labeling of Q and P directions in an "off-axis" hexagonal face for ⟨111⟩ trigonal strain. The L point at $(\frac{1}{2},\frac{\bar{1}}{2},\frac{1}{2})$ is at the center of the hexagon. β,γ designate Q lines; η,ζ designate P lines. All symmetry points are in units of $2\pi/a$.

discrepancy between our neck value and that observed is probably associated with the fact that the curvature of E vs $\vec{k}$ is quite high in this region.

B. Tetragonal strain

We may compare our results with uniaxial ⟨001⟩ tension by using Eq. (7) with ΔE and ΔE_F determined from Eq. (3). (As shown in the Appendix, $\Delta E_F = 0$ for tetragonal strain.) The scaling term analagous to the second term in Eq. (8) is now $-k_z e_{zz}$ for $\vec{k}$ components in the z direction and $-k_x e_{xx}$ for $\vec{k}$ components in the xy plane.[20] Using ΔE values from Tables VI and VII and e_{zz} and e_{xx} from Table II we obtain the "uniaxial" ⟨001⟩ Δk_F values given in Table XI. The Δk_F values in Table XI allow us to obtain a rough estimate of $d(\ln A)/d(\ln A_s)$,[21] results are given in Table XII. Agreement with Davis[15] is not as good as in the hydrostatic case. Our better agreement with the observed [001] belly value may well be fortuitous. Again, we emphasize that our areas are based on a very small number of $\vec{k}$ points as contrasted to the large number of points used by Davis.[15] It should also be noted that Davis's calculation enables him to give several other values such as the [001] rosette, [111] belly, etc.; these entities would be quite difficult for us to obtain due to the very-low-symmetry $\vec{k}$ points required.

TABLE VIII. Trigonal strain: Energy shifts at the Fermi level for $e=0.001$ in $\vec{a}_x = a_0[\hat{i} + e(\hat{j}+\hat{k})]$, etc. See text to determine the symmetry-related shifts from those listed. All energy shifts are in Ry.

Direction	State [a]	k_{radius} [b]	ΔE Perturbation
⟨110⟩	Σ_1	0.73673	−0.0008
⟨111⟩ neck	Q_α^-	0.16773	−0.0014
⟨11$\bar{1}$⟩ neck	P_ξ^+	0.16773	−0.0014
⟨1$\bar{1}$1⟩ neck	Q_β^-	0.16773	0.0008
⟨$\bar{1}$11⟩ neck	P_η^+	0.16773	0.0001

[a] For ⟨111⟩ trigonal strain, Q_α, P_ξ are any Q,P directions, respectively, in the hexagonal face normal to ⟨111⟩. The various Q,P directions in the hexagonal face normal to ⟨1$\bar{1}$1⟩ are shown in Fig. 2.

[b] Same meaning as in Table V; units of $2\pi/a_0$.

TABLE IX. Hydrostatic compression ($e=-0.005$); selected Δk_F. The units for Δk_F are $2\pi/a_0$. In the ⟨001⟩ and ⟨110⟩ directions k_F is measured from the origin (Γ); the neck k_F is measured from L.

Direction	Δk_F
⟨001⟩	0.00490
⟨110⟩	0.00237
⟨111⟩ neck	0.00226

C. Trigonal strain

As in the tetragonal case, we may compare our results with uniaxial ⟨111⟩ tension by using Eq. (7) with ΔE and ΔE_F now determined from Eq. (4). (Again, $\Delta E_F = 0$ for trigonal strain.) The scaling term is somewhat more involved than that for the tetragonal case. Using ΔE values from Tables VI and VIII and e_{xx} and e_{xy} from Table III we obtain the "uniaxial" ⟨111⟩ Δk_F values given in Table XIII. These Δk_F values allow us to obtain a rough estimate of $d(\ln A)/d(\ln A_s)$; this estimate is given in Table XIV. There appears to be qualitative agreement with the observed [111] neck value and with the calculated values of Davis[15] (except for the [001] belly).

VII. CHODOROW POTENTIAL

Table I shows that the perturbation ΔE's calculated with the Chodorow potential differ considerably from those calculated using the DFJ potential in a number of cases. Table XV shows that there is also considerable difference in ΔE near E_F. (Burdick's[22] E_F is used.) Similar comparisons for the tetragonal and trigonal cases are shown in Tables XVI and XVII, respectively. As shown by these three tables, the two potentials lead to virtually the same energy shifts in some cases (e.g., Σ_1 both shears, Q_β^- trigonal) and to somewhat different results for other cases.

VIII. DISCUSSION AND SUMMARY

For high-symmetry points (Γ,X,L) Table I indicates that energy shifts for hydrostatic compres-

TABLE X. Hydrostatic case: selected $(\Delta A/A)/\Delta P$ values in units of 10^{-7}cm^2/kg.

	This work	DFJ [a]	SOS [b] (calc.)	SOS [b] (obs.)	Templeton [c] (obs.)
[100] belly	4.20	4.53	4.51	4.5 ±0.2	4.33 ±0.03
[111] neck	12.3	15.0	20.1	17.(7) ±2.	19.4 ±0.5

[a] Reference 3.
[b] Reference 18.
[c] Reference 19.

sion with $e = -0.005$ are within about 0.001 Ry of each other for a given level for the various combinations of three different potentials and two different methods. [Γ_1 is an exception; the O'Sullivan-Switendick-Schirber (OSSS) shift is some 0.005 Ry larger than the others.] The magnitude of these high-symmetry shifts varies from about 0.001 to 0.010 Ry; all levels except L_1^u are lowered. Table VI shows that near E_F the hydrostatic shifts calculated by perturbation and by differences (using the DFJ potential in both cases) agree within about 0.0005 Ry for $e = -0.005$. Inspection of Tables XV–XVII shows that near E_F the energy shifts for the Chodorow and DFJ potentials (using the perturbation approach for both potentials) are within about 0.002 Ry of each other in the worst hydrostatic and trigonal cases and well within 0.001 Ry for the tetragonal case.

Table IV shows that the band "widths" are increased under hydrostatic compression as expected and that the "*sp*" band undergoes the expected broadening and narrowing in the appropriate directions for the shear cases. The change in the *d*-bandwidth under shear is relatively small; the direction of these small changes cannot always be predicted on the simple basis of change in atomic distance along various directions.

Comparison of Tables II and III shows that the linear combination of hydrostatic and pure shear matches the uniaxial stress results considerably better in the ⟨001⟩ case than in the ⟨111⟩ case. Since the ⟨111⟩ case requires a hydrostatic component approximately seven times that required in the ⟨001⟩ case [see Eqs. (3) and (4)], this may be an indication that the assumption of hydrostatic linearity with e is not particularly good in this range.

For the orbital area changes (Tables X, XII, and XIV) we appear to get reasonably good agreement with experiment for the [100] belly in the hydrostatic case and the [001] belly in the uniaxial ⟨001⟩ tension case. Our calculated neck orbital changes in the hydrostatic and uniaxial ⟨111⟩ tension cases differ considerably from the observed values. The circularity of the neck orbit should offset our use of a very limited number of $\vec{k}$ points in determining these orbital changes; we suspect the discrepancy is associated with the small size of the neck orbit and with the high curvature of E vs $\vec{k}$ in this region. Agreement between our calculated values and the calculated values of DFJ (hydrostatic) and Davis (uniaxial) is relatively good for the hydrostatic case (Table X); poor for the tetragonal case (Table XII); and, for the trigonal case (Table XIV), reasonably good for the [111] neck but poor for the [1$\bar{1}$1] neck and the [001] belly (for the latter case we agree with Davis in magnitude but have opposite sign).

TABLE XI. Selected Δk_F for uniaxial ⟨001⟩ tension ($e_{zz} = 0.02500$, $e_{xx} = e_{yy} = -0.010372$) using Eq. (3) of text. k_F is given in Table V. The units for Δk_F are $2\pi/a_0$.

Direction	Δk_F
⟨001⟩	−0.00179
⟨100⟩	−0.00172
⟨110⟩	−0.00364
⟨011⟩	0.00071
⟨111⟩ neck [a]	0.00217
⟨111⟩ neck [b]	−0.00202

[a] Radius from L in Q_α direction of Fig. 1.
[b] Radius from L in Q_β direction of Fig. 1.

TABLE XII. $d(lnA)/d(lnA_S)$ for uniaxial ⟨001⟩ tension (based on calculations for $e_{zz} = 0.02500$, $e_{xx} = e_{yy} = -0.010372$).

	This work	Davis [a] (calc.)	SW [b] (obs.)
[001] belly	2.7	3.6	2.4± 0.5
[100] belly	0.5	−0.3	
[111] neck	2.9	5.1	

[a] Reference 15.
[b] Reference 8.

TABLE XIII. Selected Δk_F for uniaxial ⟨111⟩ tension ($e_{xx}=e_{yy}=e_{zz}=0.01000$, $e_{xy}=e_{xz}=e_{yz}=0.02605$) using Eq. (4) of text. k_F is given in Table V. The units for Δk_F are $2\pi/a_0$.

Direction	Δk_F
⟨100⟩	−0.00982
⟨110⟩	0.00278
⟨1$\bar{1}$0⟩	−0.01369
⟨111⟩ neck [a]	0.05369
⟨1$\bar{1}$1⟩ neck [b]	−0.03094
⟨11$\bar{1}$⟩ neck [c]	−0.02051

[a] Radius from L. For the ⟨111⟩ neck symmetry dictates that all Q directions behave identically.
[b] Radius from L in the Q_β direction of Fig. 2.
[c] Radius from L in the Q_γ direction of Fig. 2.

We have shown that the modified-plane-wave method combined with a perturbation technique is a feasible approach to determining energy shifts at the Fermi level for small distortions of fcc crystals although there is some ambiguity in the shear cases due to the very limited amount of experimental values for these cases. The relatively slow convergence of the modified-plane-wave method is offset considerably by the fact that the energy shifts "converge" much more rapidly than the unperturbed energy levels. The perturbation approach is particularly appropriate for very small distortions. Thus, the best approach may be that of Juras and Segall[14] who have combined a perturbation technique with the relatively rapid Korringa-Kohn-Rostoker method.

ACKNOWLEDGMENTS

We are indebted to Dr. Harold Davis for sending us the fine-mesh potentials used in Ref. 3. It is a pleasure to acknowledge fruitful discussions with Professor E. Brown, Dr. L. V. Meisel, and Clarke Homan. We are particularly indebted to Dr. Meisel for help with the general proof given in the Appendix. The numerical computations were performed on an IBM 360-44 computer at Watervliet Arsenal; cooperation of the computer staff is acknowledged.

TABLE XIV. $d(\ln A)/d(\ln A_S)$ for uniaxial ⟨111⟩ tension (based on calculations for $e_{xx}=e_{yy}=e_{zz}=0.01000$, $e_{xy}=e_{xz}=e_{yz}=0.02605$).

	This work	Davis [a] (calc.)	SW [b] (obs.)
[001] belly	1.0	−1.2	
[111] neck	−32	−28	−44± 10
[1$\bar{1}$1] neck	14	19	

[a] Reference 15.
[b] Shoenberg and Watts, Ref. 8.

TABLE XV. Hydrostatic case: ($e=-0.005$). Comparison of ΔE at E_F using two different potentials. All entries are in Ry.

State	ΔE Chodorow $V_0(r)$ [a]	ΔE DFJ $V_0(r)$ [a]
Δ_1	−0.0031	−0.0020
Σ_1	−0.0003	0.0001
Q^-	−0.0038	−0.0019 [b]
P^+	−0.0038	−0.0019 [b]

[a] Both calculations used the $\Delta V(r)$ of DFJ.
[b] The 272-point mesh was used. (Q^- run with the 66-point mesh gave a similar value.)

APPENDIX A: SYMMETRY CONSIDERATIONS

A. Cubic crystals

We first give a simple proof[23] that, for cubic crystals, a volume-preserving "tetragonal" strain produces no change (to first order) in E_F and that

$$\sum_{\text{star of } \vec{k}} \Delta E_{k_i} = 0 \ . \tag{A1}$$

Proof. Consider simultaneously applying three tetragonal strains which single out the x, y, and z axes, respectively. The combination preserves both volume and shape (to first order) so neither E_F, any specific E_{k_i}, or $\sum_{\text{star of } \vec{k}} E_{k_i}$ changes. Since any one of the three strains may be obtained from any of the others by an operation of the cubic group, *each* strain must affect a quantity like E_F or $\sum_{\text{star of } \vec{k}} E_{k_i}$ *identically*; therefore the changes in these two quantities must be zero for each of the three strains separately. A similar argument applies for trigonal strains by simultaneously taking strains along ⟨111⟩, ⟨$\bar{1}$11⟩, ⟨1$\bar{1}$1⟩, and ⟨11$\bar{1}$⟩.

This argument also applies to the change in potential if we restrict our model to one in which the potential $V(\vec{r})$ stays spherically symmetric within a muffin-tin sphere.[24] Again, the change in $V(\vec{r})$ for the combination of three tetragonal strains

TABLE XVI. Tetragonal case ($e_{zz}=0.0050$, $e_{xx}=e_{yy}=-0.0025$). Comparison of ΔE at E_F using two different potentials. All energies are in Ry.

Direction	State [a]	ΔE Chodorow $V_0(r)$	ΔE DFJ $V_0(r)$
⟨001⟩	Δ_1	−0.0059(0)	−0.0064(5)
⟨110⟩	Σ_1	0.0021(5)	0.0019(0)
⟨111⟩ neck	Q_α^-	~0.0	−0.0001(2)

[a] For ⟨001⟩ tetragonal strain, the various directions in the hexagonal face normal to ⟨111⟩ are shown in Fig. 1.

TABLE XVII. Trigonal case ($e_{xy} = e_{xz} = e_{yz} = 0.005$). Comparison of ΔE at E_F using two different potentials. All energies are in Ry.

Direction	State [a]	ΔE Chodorow $V_0(r)$	ΔE DFJ $V_0(r)$
⟨110⟩	Σ_1	−0.0043(5)	−0.0041(0)
⟨111⟩ neck	Q_α	−0.0089(5)	−0.0073(5)
⟨1$\bar{1}$1⟩ neck	Q_β	0.0040(0)	0.0039(5)

[a] For ⟨111⟩ trigonal strain, Q_α is any Q direction in the hexagonal face normal to ⟨111⟩. The various directions in the hexagonal face normal to ⟨1$\bar{1}$1⟩ are shown in Fig. 2.

must be zero. For *spherically symmetric* $V(r)$ the change due to *each* strain must be identical, so that $\Delta V(r) = 0$ for each.

It should be noted that no more information can be obtained from the Wigner-Eckart theorem than from standard compatibility tables combined with the "star-of-$\vec{k}$" theorem above. (The Wigner-Eckart theorem merely corroborates the information that some shifts are *probably* not equal to zero.)

B. General

It is of interest to extend the arguments in the previous section to all classes of crystals and to determine which strains result in preservation of E_F and $\sum_{\text{star of } \vec{k}} E_{k_i}$. One is led to the following theorem: For any crystal, ΔE_F and $\sum_{\text{star of } \vec{k}} \Delta E_{k_i}$ equal zero (to first order) for any strain which does not contain a Γ_1 component.

Proof. Define

$$\Pi^i_\alpha \equiv \frac{l_i}{|G|} \sum_R D^i_{\alpha\alpha}(R) P_R \ , \tag{A2}$$

where $D^i_{\alpha\alpha}(R)$ is the $\alpha\alpha$ element of the matrix representing R in the ith irreducible representation, l_i is the dimensionality of the representation and $|G|$ is the number of members in the covering group of the crystal. We may write an arbitrary strain tensor $\underline{e}$ as

$$\underline{e} = \sum_{i,\alpha} \Pi^i_\alpha \underline{e} = \sum_{i,\alpha} c_{i\alpha} \underline{e}^{i\alpha} \ , \tag{A3}$$

i.e., decomposition of the desired strain $\underline{e}$ into a linear sum of components, each transforming like one partner of one irreducible representation, is always possible; further, each $\underline{e}^{i\alpha}$ may be written

$$\underline{e}^{i\alpha} = \Pi^i_\alpha \underline{\theta}^{i\alpha} . \tag{A4}$$

Applying Π^1_1 to both sides of Eq. (A3) gives

$$\Pi^1_1 \underline{e} = \sum_{i,\alpha} c_{i\alpha} \Pi^1_1 \Pi^i_\alpha \underline{\theta}^{i\alpha} = c_{11} \underline{e}^{11}$$

since $\Pi^j_\beta \Pi^i_\alpha = \delta_{ij} \delta_{\alpha\beta} \Pi^j_\beta$.

Thus

$$\Pi^1_1 \underline{e} = 0 \text{ for } c_{11} = 0 \ , \quad \neq 0 \text{ for } c_{11} \neq 0 \ . \tag{A5}$$

Since $D^1_{11}(R) = 1$ for all R in G, Π^1_1 applied to $\underline{e}$ is equivalent to applying all the operations of G to $\underline{e}$ (times a factor $1/|G|$). Since each operation merely rotates the strain, ΔE_F (and $\sum_{\text{star of } \vec{k}} \Delta E_{k_i}$) is the same for each such rotated strain as for $\underline{e}$; thus, from Eq. (A5), these quantities are zero when $c_{11} = 0$, i.e., when the original strain $\underline{e}$ does not contain a Γ_1 component.

As a corollary it follows that: (i) For *cubic* crystals $\Delta V = 0$, where V is the volume, is the necessary and sufficient condition to have ΔE_F and $\sum_{\text{star of } \vec{k}} \Delta E_{k_i} = 0$. (ii) For *noncubic* crystals $\Delta V = 0$ is only a necessary condition.

[1] A. Marcus Gray, D. M. Gray, and E. Brown, Phys. Rev. B 11, 1475 (1975).

[2] A preliminary report of our results was given at the Conference on Electronic Properties of Solids under High Pressure, Leuven, Belgium, 1–5 September, 1975 (unpublished). See Europhys. Conf. Abstracts, 1A, 17 (1975); (abstract only).

[3] H. L. Davis, J. S. Faulkner, and H. W. Joy, Phys. Rev. 167, 601 (1968).

[4] P. O. Löwdin, Adv. Phys. 5, 1 (1956); L. F. Mattheiss, Phys. Rev. 133, A1399 (1964).

[5] R. E. Watson, Phys. Rev. 119, 1934 (1960).

[6] $rV(r)$ for some selected mesh points for a, 0.995a and 0.99a as well as $\overline{V}$ for the three cases are tabulated in Ref. 3. The explicit potential used in the present paper is obtainable from us.

[7] W. B. Pearson, *A Handbook of Lattice Spacings and Structures of Metals and Alloys* (Pergamon, New York, 1958).

[8] D. Shoenberg and B. R. Watts, Philos. Mag. 15, 1275 (1967).

[9] R. Griessen and R. S. Sorbello, J. Low Temp. Phys. 16, 237 (1974).

[10] M. I. Chodorow, Ph.D. thesis (MIT, 1939) (unpublished).

[11] W. J. O'Sullivan, A. C. Switendick, and J. E. Schirber, Phys. Status Solidi B 68, K29 (1975). This is a Korringa-Kohn-Rostoker calculation with potentials derived from Herman-Skillman atomic calculations by means of the Löwdin-Mattheiss prescription.

[12] L. P. Bouckaert, R. Smoluchowski, and E. Wigner, Phys. Rev. 50, 58 (1936).

[13] Both X_5 and L_3 have been rerun using the 272-point

mesh and a large number of symmetrized plane waves (62 and 60, respectively). While E^0 dropped 0.018 Ry for X_5 and 0.021 Ry for L_3^u, the ΔE values changed by only 6×10^{-5} Ry in both cases. We have also calculated X_5 by differences (with the 272-point mesh) obtaining a shift of -0.0010 Ry, i.e., identical to that obtained by perturbation.

[14]G. E. Juras and B. Segall, Phys. Rev. Lett. 29, 1246 (1972); Surf. Sci. 37, 929 (1973).

[15]H. L. Davis in Proceedings of Colloque International du C.N.R.S. sur les Propriétés Physiques des Solides sous Pression, Grenoble, (1969), p. 123.

[16]Strain components are as defined by Juras and Segall (Ref. 14). This is consistent with I. This also corresponds to Kittel's notation [C. Kittel, *Introduction to Solid State Physics*, 2nd ed. (Wiley, New York, 1956)], except for the trigonal case where Kittel's $\frac{1}{2}e$ is replaced by e.

[17]The experimental volume compressibility, $(\Delta V/V)/\Delta P = -6.907\times10^{-7}$ cm^2/kg [W. C. Overton and J. Gaffney, Phys. Rev. 98, 969 (1955)], is used in the present paper and in Refs. 3 and 18.

[18]J. E. Schirber and W. J. O'Sullivan in Proceedings of Colloque International du C.N.R.S. sur les Propriétés Physiques des Solides sous Pression, Grenoble, 1969; p. 113.

[19]I. M. Templeton, Can. J. Phys. 52, 1628 (1974).

[20]For the neck radius, scaling is somewhat more involved.

[21]A is the area of the appropriate orbit. A_s is the diametral area of a free-electron sphere whose volume remains exactly half that of the Brillouin zone.

[22]G. A. Burdick, Phys. Rev. 129, 138 (1963). We used the following for k_F: Δ_1, $k_z = 0.816$; Σ_1, $k_x = k_y = 0.524$; Q^-, P^+, radius from $L = 0.1273$.

[23]This is essentially the proof given in I; the proof there was more cumbersome as we were also showing the applicability of the Wigner-Eckart theorem.

[24]The fact that $\Delta V(r) = 0$ for such a model was first noted by Juras and Segall in the first paper cited in Ref. 14.